

Macrofacet Theory for Gaussian Process Statistical Surfaces

MINGHAO HUANG, University of California Santa Barbara, United States of America

YUANG CUI, Anhui Science and Technology University, China

BEIBEI WANG, Nanjing University, China

LINGQI YAN, Mohamed bin Zayed University of Artificial Intelligence, United Arab Emirates

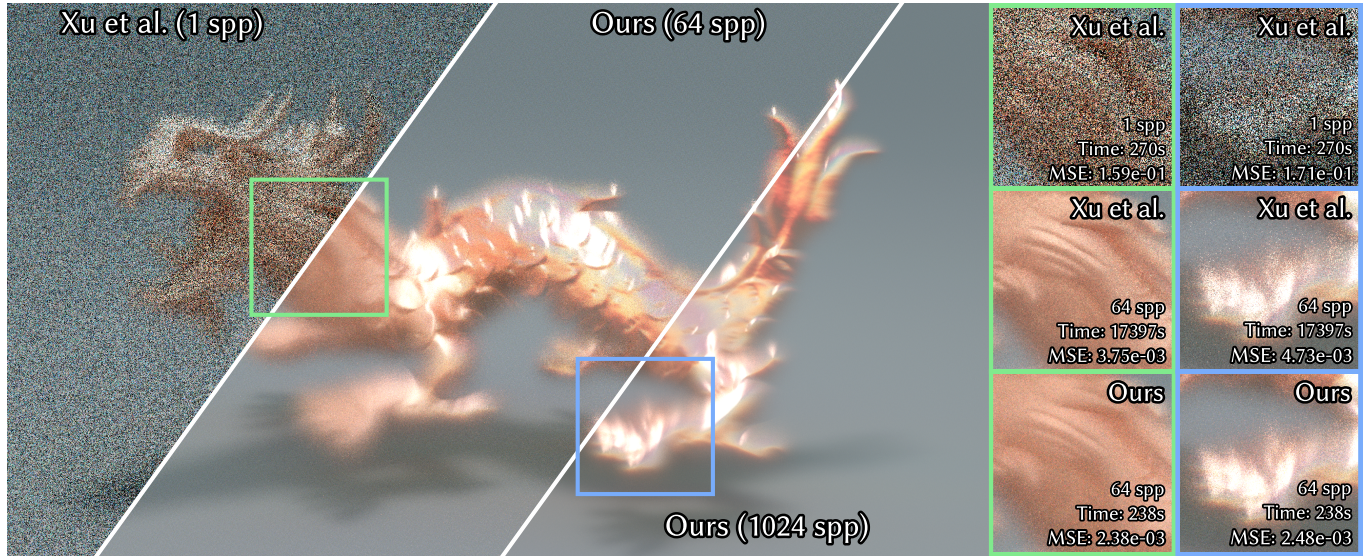


Fig. 1. Our macrofacet theory connects microfacet theory and Gaussian process implicit surfaces theoretically. We use classic exponential media to represent surfaces, volumes and in-betweens without realization of Gaussian processes. We compare our method with previous work by Xu et al. [2025] at equal time and equal samples per pixel (spp) showing a significant improvement in rendering efficiency. The variance increases from top to bottom, while the correlation increases from left to right. The rightmost two columns show magnified insets comparing two approaches. The MSE in each inset is computed separately, while the time is the total rendering time of the image.

We present macrofacet theory, taking microfacet theory from micro-space to macro-space by stretching a surface to a volume to make it have microfacet characteristic in macro-space. In this way, we have a macroscopic microfacet formulation that uses a classic exponential participating medium. Meanwhile, we observe that traditional microfacet models are equivalent to Gaussian processes in definition but ignore the correlation along the geometric normal of macro-surface. We extend microfacet theory so that macrofacet can handle this problem and represent Gaussian process implicit surfaces in a statistical way. As a result, our approach converts Gaussian process implicit surfaces into classic exponential media to render surfaces, volumes and in-betweens without realization. These enable efficient rendering with performance improvement compared to realization-based approaches, while bridging microfacet models and Gaussian processes theoretically. Moreover, our approach is easy to implement and friendly for artists.

CCS Concepts: • **Computing methodologies** → **Reflectance modeling**.

Additional Key Words and Phrases: volumetric light transport, stochastic processes, implicit surfaces, microfacet theory, microflake theory

Authors' Contact Information: [Minghao Huang](mailto:minghao_huang@ucsb.edu), minghao_huang@ucsb.edu, University of California Santa Barbara, Santa Barbara, United States of America; [Yuang Cui](mailto:yuangcui@outlook.com), yuangcui@outlook.com, Anhui Science and Technology University, Anhui, China; [Beibei Wang](mailto:beibei.wang@nju.edu.cn), beibei.wang@nju.edu.cn, Nanjing University, Nanjing, China; [Lingqi Yan](mailto:lingqi.yan@mbzuai.ac.ae), lingqi.yan@mbzuai.ac.ae, Mohamed bin Zayed University of Artificial Intelligence, Abu Dhabi, United Arab Emirates.

1 INTRODUCTION

Surface and volume have traditionally been treated as two distinct fields in rendering. Surface appearance is typically defined by explicit geometries, while volumetric appearance is modeled through stochastic light transport governed by extinction and scattering with particles. This separation has led to two largely independent theoretical and practical pipelines, despite the fact that many real-world appearances such as porous materials and partially coherent structures—lie somewhere in between. Bridging the gap between surface and volumetric appearance is important both theoretically and practically. From a theoretical perspective, it raises fundamental questions about how geometries and particles should be represented across scales. From a practical standpoint, a unified treatment promises more robust and efficient rendering of materials without manually switching between surface and volumetric rendering techniques.

There exist methods using microflake theory explaining microfacet theory to unify surface and volume [Dupuy et al. 2016; Heitz et al. 2016]. However, they are still in micro-space and assume that the distribution of microfacets is a height field, neglecting the correlation of microfacets on the geometric normal of macro-surface. This leads to a failure in representing materials whose micro-geometries

have holes and overlaps, like porous materials. What’s more, handling correlation in participating media is already a difficult problem [Bitterli et al. 2018; Jarabo et al. 2018].

In fact, the traditional microfacet model is defined as a 2D Gaussian process on the xy -plane which is the macro-surface. When moved to 3D, it becomes a fully anisotropic 3D Gaussian process where the correlation on the geometric normal of macro-surface, that is, the z -axis, is infinity, resulting in a height field. When the correlation on the z -axis goes from infinity to finitely low, the Gaussian process implicit surface changes from a height field to a porous micro-geometry. Therefore, rendering a surface-type Gaussian process is essentially rendering a microfacet surface [Seyb et al. 2024; Xu et al. 2025]. Nevertheless, rendering Gaussian process implicit surfaces requires realizations of Gaussian processes, which cost a large amount of time and is hard to implement.

We propose macrofacet theory to: 1) extend microfacet theory to describe 3D Gaussian processes; 2) represent Gaussian process implicit surfaces in classic exponential media statistically. Therefore, we unify surface, volume and in-between representations. We extend a macro-surface to a volume in order to transform microfacet theory to microflake theory in macro-space. We derive the extinction coefficient and phase function of microfacet in macro-space according to microfacet theory. On the basis of definition of 3D Gaussian processes, we also analytically compute the transmittance, normals’ distribution function and phase function of the corresponding classic exponential media within a de-correlation assumption. As a consequence, we can render macrofacet by any classic exponential media rendering techniques *without realization*. Hence, it is very fast and friendly for implementation and artists.

2 RELATED WORK

2.1 Gaussian Processes

Gaussian processes are used to model distributions over functions. They are widely used in machine learning [Rasmussen and Williams 2005], signal processing [Ricciardi and Sato 1986] and other areas. In computer graphics, they have been applied for surface reconstruction [Martens et al. 2017; Williams and Fitzgibbon 2007], where Gaussian process is conditioned on a set of point observations and the surface is extracted from the zero-crossing of the Gaussian process mean.

Seyb et al. [2024] propose a light transport framework using Gaussian processes to represent stochastic geometries. They realize Gaussian processes to obtain implicit surfaces on-the-fly and ensemble average over the light transport on these realizations. This unifies the representations of surfaces, volumes and even the in-betweens which shows the macro-scale uncertainty. However, because of the heavy computation of realizations, it requires a lot of time to render results in spite of their Renewal and Renewal+ model. Xu et al. [2025] introduce sparse convolution noise to approximate Gaussian processes to reduce the computation of realizations. They also utilize next-event estimation to further reduce noise. Nevertheless, both of them require a large amount of realizations of Gaussian processes while ray marching, resulting in a low efficiency. And it is hard to implement for current rendering engines. Our macrofacet

is a classic medium, so it is easily implemented in current rendering engines.

2.2 Microfacet Surface

Cook and Torrance [1982] propose the microfacet model for reflection on rough surfaces. They average over reflectance from a statistical representation of the micro-geometry of surface consisting of specular microfacets. This model is then extended to rough dielectrics [Stam 2001]. Walter et al. [2007] use the Smith’s assumption [Smith 1967] to apply more normal distribution functions to the model, such as the GGX distribution.

Different normal distribution functions result in different appearances of the surface. In the beginning, the Beckmann distribution [Beckmann 1965; Cook and Torrance 1982] is widely used. Trowbridge and Reitz [1975] propose a distribution on half-ellipsoids. Walter et al. [2007] adopt it as the GGX distribution to achieve a more realistic result.

Typical microfacet model only calculates the reflectance from a single bounce of a light ray intersecting the micro-geometry of surface, which results in energy loss, especially when the roughness is high. Heitz et al. [2016] treat microfacets as randomly distributed microflakes using a height distribution so that they can trace multiple bounce rays in a random walk solution. Wang et al. [2022] assume that microflakes are position-free to avoid noise from the height distribution. Cui et al. [2023] further introduces the invariance principle to generalize the shadow masking function from a single bounce to an entire path to achieve less noise. Since we use volume to represent materials, our macrofacet supports multiple bounce naturally.

2.3 Participating Media

The standard form of radiative transport equation [van de Hulst 1957] is usually stated for spherical or randomly oriented particles, which is not the case for anisotropic media. Jakob et al. [2010] propose a physically-based radiative transfer framework called microflake for anisotropic media [Kuščer and Summerfield 1969; Williams 1978]. The volume scattering model within this framework is analogous to the microfacet model, using oriented non-spherical particles. It is widely used in woven [Zhao et al. 2011, 2012] and cloth [Schröder et al. 2012] materials. Heitz et al. [2015] introduce the SGGX distribution to represent spatially-varying properties of anisotropic media based on microflake theory. Dupuy et al. [2016] assumes a semi-infinite homogeneous exponential-free-path medium to unify microfacet and microflake theories. However, this assumption is still in micro-space and does not consider the case of 3D Gaussian processes where correlation on the z -axis is finite. Our macrofacet theory unifies microfacet and microflake theories in macro-space and connect Gaussian process implicit surfaces to classic participating media.

3 BACKGROUND AND OVERVIEW

In this section, we introduce the background knowledge of Gaussian processes, microfacet and microflake theories, and give an overview of our proposed macrofacet theory to connect them. The notations that will be used throughout our paper are listed in Table 1.

Table 1. Notations.

Mathematical notation	
Ω	full spherical domain
μ	mean
σ^2	variance
l	correlation
κ	covariance kernel
$\phi(x; \mu, \sigma^2)$	Gaussian probability density function with mean μ and variance σ^2
$\Phi(x; \mu, \sigma^2)$	Gaussian cumulative density function with mean μ and variance σ^2
$\omega_1 \cdot \omega_2$	dot product
$ \omega_1 \cdot \omega_2 $	absolute value of the dot product
$\langle \omega_1, \omega_2 \rangle$	clamped dot product
Physical quantities	
f	signed distance field
g	gradient of a signed distance field
α	roughness
$\omega_g = (0, 0, 1)$	geometric normal
ω_m	microfacet normal
ω_i	incident direction
ω_o	outgoing direction
h	microsurface height on z-axis
$P^1(h)$	height distribution
$C^1(h)$	cumulative height distribution
$\Lambda(\omega)$	the Smith Lambda function
$D(\omega_m)$	normal distribution function
$F(\omega_o, \omega_h)$	Fresnel term
$D_{\omega_o}(\omega_m)$	visible normals' distribution
$\rho(h)$	Microflake density
$\sigma(\omega_o)$	Microflake projected area
$\sigma_t(\omega_o, h)$	Microflake extinction coefficient
$p(\omega_o, \omega_i)$	Microflake phase function

3.1 Gaussian Processes

A Gaussian process $f(\mathbf{x}) \sim \mathcal{GP}(\mu(\mathbf{x}), \kappa(\mathbf{x}, \mathbf{y}))_{\mathbb{R}^3}$ is a distribution over functions f characterized by the mean function $\mu(\mathbf{x}) = \mathbb{E}(f(\mathbf{x}))$ and the covariance kernel $\kappa(\mathbf{x}, \mathbf{y}) = \text{Cov}(f(\mathbf{x}), f(\mathbf{y}))$. There are many types of covariance kernels. We focus on the squared exponential (SE) kernel, which is a stationary kernel and defined as

$$\kappa(\mathbf{x}, \mathbf{y}) = \sigma^2 \exp\left(-\frac{1}{2}(\mathbf{x} - \mathbf{y})^T \text{diag}(l_x^2, l_y^2, l_z^2)^{-1}(\mathbf{x} - \mathbf{y})\right), \quad (1)$$

where σ^2 is the variance. l_x , l_y and l_z are the correlation on the x , y and z axis respectively. When $l_x = l_y = l_z$, the covariance kernel is isotropic. Otherwise, it is anisotropic. The variance and correlation are independent variables.

A Gaussian Process Implicit Surface (GPIS) is the zero level set of a Gaussian process. This implicit surface is stochastic: every realization f drawn from the Gaussian process generates a different surface where $f(\mathbf{x}) = 0$. Within each realization, the light transport is given by the classical rendering equation [Kajiya 1986]

$$L^f(\mathbf{x}, \omega_o) = \int_{\Omega} \rho^f(\mathbf{x}_s^f) L^f(\mathbf{x}_s^f, \omega_i) d\omega_i, \quad (2)$$

where $L^f(\mathbf{x}, \omega_o)$ is the radiance arriving at point \mathbf{x} from direction ω_o . \mathbf{x}_s^f is the closest intersection along the ray with the direction ω_o starting from \mathbf{x} . $\rho^f(\mathbf{x}_s^f)$ is the cosine-weighted BRDF.

The total radiance received is the ensemble average over all possible realizations

$$\langle L^f(\mathbf{x}, \omega) \rangle_{\zeta} = \int_{\mathcal{GP}} L^f(\mathbf{x}, \omega) d\gamma(f | \zeta), \quad (3)$$

where ζ represents a set of constraints and $\gamma(f | \zeta)$ is the classic Wiener measure, the probability density of sampling $f \sim \mathcal{GP}|_{\zeta}$.

GPIS can be surface-type, volume-type or even in-between type determined by its mean function and covariance kernel [Seyb et al. 2024]. In-betweens present macro-scale uncertainty as ‘‘fuzziness’’. When the mean function is the signed distance field (SDF), GPIS appears like a surface or an in-between. When the mean function is a constant, it appears like a homogeneous medium. The covariance kernel not only affects the roughness but also the fuzziness of the appearance. The roughness can be derived from the second derivative of the covariance kernel [Pharr et al. 2016]. Here is for the SE kernel:

$$\alpha = \sqrt{-2\kappa''(0)} = \sqrt{2} \frac{\sigma}{l}. \quad (4)$$

3.2 Microfacet Theory

The microfacet theory describes a statistical model at micro-scale with a height distribution $P^1(h)$ and a normal distribution $D(\omega_m)$ of micro-surfaces. The Smith’s assumption [Smith 1967] de-correlates $P^1(h)$ and $D(\omega_m)$, so we can choose them independently. In order to map our macrofacet theory to GPIS, we choose the Gaussian distribution with variance σ^2 for $P^1(h)$:

$$P^1(h) = \phi(h; 0, \sigma^2) = \frac{1}{\sqrt{2\pi}\sigma} e^{-\frac{h^2}{2\sigma^2}}, \quad (5)$$

where $h \in (-\infty, +\infty)$ and $h = 0$ means the average plane of the surface. There are many types of normal distributions $D(\omega_m)$, usually referred to NDF. Two mainly used are Beckmann and GGX distributions [Walter et al. 2007]. They are defined by the roughness α equivalent to Equation 4.

Dupuy et al. [2016] and Heitz et al. [2016] use participating media [Heitz et al. 2015; Jakob et al. 2010] to describe microfacet theory. The density of the volume associated with a Smith microfacet surface is defined as²

$$\rho(h) = \frac{P^1(h)}{C^1(h)}. \quad (6)$$

The corresponding projected area is

$$\sigma(\omega_o) = \int_{\Omega} \langle -\omega_o, \omega_m \rangle D(\omega_m) d\omega_m = \Lambda(\omega_o) \cos \theta_o, \quad (7)$$

where $\cos \theta_o$ is the cosine of outgoing direction ω_o and geometric normal ω_g . We clarify that the outgoing direction ω_o is always pointing to the origin of the incoming direction ω_i . And the extinction

¹The height distribution can be chosen arbitrary [Bitterli and d’Eon 2022; Cui et al. 2023; Heitz et al. 2016; Wang et al. 2022]. However, the SDF distribution of any point in the space is a Gaussian distribution if it is generated by a Gaussian process. Therefore, we choose the Gaussian distribution in order to match our method to GPIS.

²The density is monotonic instead of symmetric no matter what height distribution is chosen.

coefficient is the product of microflake density and projected area:

$$\sigma_t(\omega_o, h) = \rho(h)\sigma(\omega_o) = \frac{P^1(h)}{C^1(h)}\Lambda(\omega_o)\cos\theta_o. \quad (8)$$

As we know the extinction coefficient, we can compute the transmittance which is the remaining energy when a ray travel at distance t in the medium:

$$\text{Tr}(\omega_o, t) = \exp\left(-\int_0^t \sigma_t(\omega_o, h(t))dt\right). \quad (9)$$

The phase function of a volume depends, describing how a ray is scattered in the medium, depends on the its material. In this paper, we focus on the conductor material, which we can obtain a conductor phase function:

$$p(\omega_o, \omega_i) = \frac{F(-\omega_o, \omega_h)D_{\omega_o}(\omega_h)}{4|-\omega_o \cdot \omega_h|}, \quad (10)$$

where $\omega_h = \frac{-\omega_o + \omega_i}{\|-\omega_o + \omega_i\|}$ is the half vector. The visible normals' distribution (vNDF) $D_{\omega_o}(\omega_m)$ is defined as

$$D_{\omega_o}(\omega_m) = \frac{\langle -\omega_o, \omega_m \rangle D(\omega_m)}{\int_{\Omega} \langle -\omega_o, \omega_m \rangle D(\omega_m) d\omega_m} = \frac{\langle -\omega_o, \omega_m \rangle D(\omega_m)}{\Lambda(\omega_o)\cos\theta_o}. \quad (11)$$

This phase function satisfies both reciprocity and energy conservation. According to Equation 10 and Equation 11, we know the relation between NDF and phase function. Therefore, when we derive phase function for macrofacet later, we need to know NDF.

3.3 Overview

The in-between GPIS is a new type of appearance introducing the macro-scale uncertainty, or in other words, fuzziness. However, current GPIS rendering techniques require realizations of a GPIS [Seyb et al. 2024; Xu et al. 2025], which costs tons of time and is different from the traditional rendering framework. We want to use volumetric rendering technique to achieve a similar appearance to avoid realizations and be applicable for traditional rendering engine. Microfacet theory assumes that there are many micro-surfaces floating in the micro-space. We proposes macrofacet theory, assuming that these micro-surfaces floating in macro-space, like a microflake volume, so that we can get a ‘‘fuzzy’’ appearance similar to in-between GPIS naturally. What’s more, macrofacet theory builds a bridge connecting microfacet theory to GPIS and can be mapped to GPIS, meaning that we can render GPIS in a volumetric rendering way to reduce lots of time. Since we consider the statistical surface instead of the actual implicit surface realized by a Gaussian process, we call it *Gaussian process statistical surface (GPSS)*.

4 MACROFACET

In this section, we propose the macrofacet theory and show how it can connect microfacet theory and GPIS.

The core idea of macrofacet is first taking micro-surfaces from micro-space to macro-space and maintaining the total number of micro-surfaces. Imaging that we have a volume containing many particles, how we stretch this volume does not change the total number of particles. In order to achieve this, we extend the original macro-surface in z -axis to get a shell. The distance from the upper/lower face to the original macro-surface $f(\mathbf{x}) = 0$ is 3σ , where σ^2 is the variance of height distribution of micro-surfaces described

in Equation 5. Since the probability outside $[-3\sigma, 3\sigma]$ of a Gaussian distribution is low enough to be ignored, we can claim that the shell contains all micro-surfaces. The space inside the shell is a microflake volume. Then the micro-surfaces in micro-space become microflakes in macro-space. Figure 2 shows the extension.

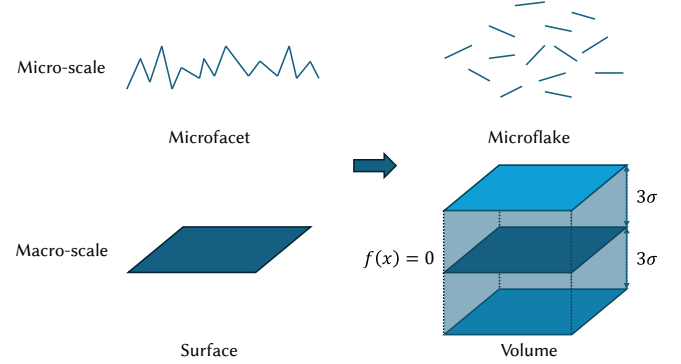


Fig. 2. Extension of a macro-surface. The top row illustrates the micro-scale extension of macrofacet, while the bottom row illustrates the macro-scale extension of macrofacet. Originally, the object is a surface at macro-scale and microfacet at micro-scale. We stretch the macro-surface upwards and downwards by the length of 3σ . In this way, the macro-surface becomes a shell volume. At the same time, microfacets become microflakes floating inside the shell.

Then, the height h in micro-space is mapped to SDF f in macro-space [Seyb et al. 2024]. Therefore, we perform parameter conversion in Equation 6 and Equation 8:

$$\rho(f) = \frac{P^1(f)}{C^1(f)} = \frac{\phi(f; 0, \sigma^2)}{\Phi(f; 0, \sigma^2)}, \quad (12)$$

$$\sigma_t(\omega_o, f) = \frac{P^1(f)}{C^1(f)}\Lambda(\omega_o)\cos\theta_o. \quad (13)$$

And the normal in macro-space is the normalized gradient of SDF. The phase function follows Equation 10. In this way, when $\sigma \rightarrow 0$, the shell degenerates to a surface and appears the same as a microfacet surface.

4.1 Height Field Macrofacet

If we choose Beckmann distribution as macrofacet NDF, it will be a fully anisotropic GPIS where the correlation on the z -axis l_z is infinity. In fact, Beckmann distribution is a 2D Gaussian process with an SE kernel on the xy -plane [Beckmann 1965]. The roughness on the x -axis α_x and y -axis α_y are defined as $\sqrt{2}\sigma/l_x$ and $\sqrt{2}\sigma/l_y$, respectively, which are the same as Equation 4. When we put this 2D Gaussian process into 3D, the correlation on the z -axis will be infinity because there is only one zero-crossing along the same z -axis, meaning that the GPIS is a height field, consistent with the microfacet assumption.

In order to render a fully anisotropic GPIS in a classic exponential media, we need to consider the phase function and transmittance of the media. Seyb et al. [2024] show that NDF of a fully anisotropic GPIS is the same as Beckmann distribution, so we can use Beckmann distribution to calculate the phase function. And calculating the

transmittance of a GPIS is indeed calculating the shadow masking term $G_1(\omega_o)$. Smith [1967] uses $S(h, p_0, q_0, \omega_o)$, or $S(F, \omega_o)$ for short, to denote the probability that a point F on a fully anisotropic GPIS, of given height h above the average plane, and with local slopes p_0, q_0 , will not lie in shadow when the surface is illuminated with an incident light ray ω_o . It can be written as the limit

$$S(F, \omega_o) = \lim_{t \rightarrow \infty} S(F, \omega_o, t), \quad (14)$$

where $S(F, \omega_o, t)$ is the probability that no part of the surface between F and $F + t\omega_o$ will intersect the ray ω_o . The meaning of $S(F, \omega_o, t)$ is equivalent to the transmittance of the ray ω_o originating from F and advancing t . It can be derived to

$$S(F, \omega_o, t) = S(F, \omega_o, 0) \exp\left(-\int_0^t \sigma_t(\omega_o, t) dt\right), \quad (15)$$

where $\sigma_t(\omega_o, t)$ is exactly the extinction coefficient of the volume. Smith [1967] neglects correlation between the height and slopes at F and those at $F + t\omega_o$ in order to simply calculate $\sigma_t(\omega_o, t)$:

$$\sigma_t(\omega_o, t) = \frac{\phi(h + t \cos \theta_o; 0, \sigma^2)}{\Phi(h + t \cos \theta_o; 0, \sigma^2)} \Lambda(\omega_o) \cos \theta_o, \quad (16)$$

which is the same as Equation 8 in micro-space and Equation 13 in macro-space. Therefore, the extinction coefficient in Equation 13 is consistent with a GPIS. We draw a picture comparing the transmittance between Beckmann macrofacet, a fully anisotropic GPIS and an isotropic GPIS in Figure 3. It shows that Beckmann macrofacet and the fully anisotropic GPIS are almost the same. Above all, due to the consistency with the phase function and transmittance, Beckmann macrofacet is the same as a fully anisotropic GPIS.

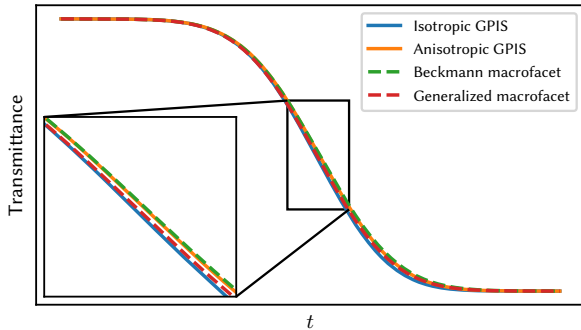


Fig. 3. Comparison of transmittance between macrofacets and GPISes. The figure shows the transmittance of a ray intersecting macrofacet and GPIS planes at a 45° incident angle, where $-\omega_o \cdot \omega_g = \sqrt{2}/2$. The transmittance of Beckmann macrofacet (green dashed line) matches the one of fully anisotropic GPIS (orange line) very well. The transmittance of generalized macrofacet (red dashed line) matches the one of isotropic GPIS (blue line) well in the first half, but has a slight difference in the latter half, probably due to the de-correlated assumption.

Besides, with the Smith's assumption [Smith 1967], we can choose arbitrary NDF ignoring the density distribution of microflakes. This, instead of choosing different covariance kernels of Gaussian processes, makes macrofacet more flexible and easier for artists to understand the appearance of macrofacet. For example, we can choose GGX distribution as macrofacet NDF to get a more realistic

appearance than Beckmann distribution when the shell degenerates to a surface.

4.2 Generalized Macrofacet

When the correlation on the z -axis is finite, the GPIS is no longer a height field, shown in Figure 4. There are multiple zero-crossings along the same z -axis. And there are micro-surface normals pointing downward, forming a microfacet surface with holes and overlaps, which is difficult to handle. Traditional microfacet theory does not handle this situation and cannot connect to a general GPIS because it only assumes a height field. In this case, we still focus on two important properties of a classic exponential media - transmittance, or extinction coefficient, and phase function.

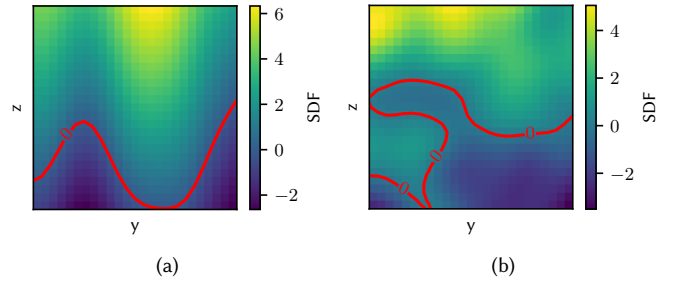


Fig. 4. GPISes with different correlations on the z -axis. These two figures show SDFs in yz -slices of realizations of (a) a strongly anisotropic GPIS with $L_z = 10$ and (b) an isotropic one with $L_z = 1$. The red lines are the zero level sets, indeed the realizations of GPISes. We can see that (a) the strongly anisotropic GPIS is a height field, while (b) the isotropic one is no longer a height field, having normals pointing downward.

Extinction coefficient. In order to deal with these problems, we first extend our transmittance calculation from 2D to 3D. Suppose \mathbf{x} is a point in the macro-space. $f(\mathbf{x})$ is the SDF and $f(\mathbf{x}) \sim \mathcal{GP}(\mu(\mathbf{x}), \kappa(\mathbf{x}, \mathbf{y}))_{\mathbb{R}^3}$, where $\mu(\mathbf{x}) = z$ and $\kappa(\mathbf{x}, \mathbf{y})$ is Equation 1. $g(\mathbf{x}) = \nabla f(\mathbf{x})$ is the gradient. Let $\mathbf{x}_0 = (0, 0, z_0)$ be the initial point. $\omega_o = (\sin \theta_o \cos \phi_o, \sin \theta_o \sin \phi_o, \cos \theta_o)$ is the unit directional vector. t is the travel distance. We denote the probability that a point \mathbf{x}_0 on a GPIS, of given SDF $f(\mathbf{x}_0)$, and with local gradient $g(\mathbf{x}_0)$, will not lie in shadow when the surface is illuminated with an incident light ray ω_o as $S(f(\mathbf{x}_0), g(\mathbf{x}_0), \omega_o)$, or $S(\mathbf{x}_0, \omega_o)$ for short. It can be written as the limit

$$S(\mathbf{x}_0, \omega_o) = \lim_{t \rightarrow \infty} S(\mathbf{x}_0, \omega_o, t), \quad (17)$$

where $S(\mathbf{x}_0, \omega_o, t)$ is the probability that no part of the GPIS between \mathbf{x}_0 and $\mathbf{x}_0 + t\omega_o$ will intersect the ray ω_o . Then $S(\mathbf{x}_0, \omega_o, t)$ is the transmittance of the ray ω_o originating from \mathbf{x}_0 and advancing t . The detailed derivation is shown in the supplemental material. It can be transformed to a volumetric light transport equation:

$$S(\mathbf{x}_0, \omega_o, t) = S(\mathbf{x}_0, \omega_o, 0) \exp\left(-\int_0^t \sigma_t(\omega_o, t) dt\right), \quad (18)$$

where $\sigma_t(\omega_o, t)$ is the extinction coefficient. Similar to the Smith's assumption [Smith 1967], we suppose that the SDF and gradient at

\mathbf{x}_0 and those at $\mathbf{x}_0 + t\omega_o$ are independent, so that we can get:

$$\begin{aligned}\sigma_t(\omega_o, t) &= \rho(t)\sigma(\omega_o), \\ \rho(t) &= \frac{\phi(z_0 + t \cos \theta_o; 0, \sigma^2)}{\Phi(z_0 + t \cos \theta_o; 0, \sigma^2)}, \\ \sigma(\omega_o) &= \Lambda(\omega_o) \cos \theta_o,\end{aligned}\quad (19)$$

$$\begin{aligned}\Lambda(\omega_o) &= \frac{1}{2a\sqrt{\pi}} e^{-a^2} + \frac{1}{2}(\text{erf}(a) - 1), \\ a &= \frac{\cos \theta_o}{\sqrt{\alpha_x^2 \sin^2 \theta_o \cos^2 \phi_o + \alpha_y^2 \sin^2 \theta_o \sin^2 \phi_o + \alpha_z^2 \cos^2 \theta_o}},\end{aligned}\quad (20)$$

where erf is the error function. Here we define $\alpha_z = \sqrt{2}\sigma/l_z$ as the ‘‘roughness’’ on the z -axis. When $\alpha_z \rightarrow 0$, that is, $l_z \rightarrow \infty$, the GPIS is a height field, and Equation 20 degenerates to the Beckmann version of Smith Lambda function. Interestingly, we can see that the form of extinction coefficient is the same as Equation 13, where $\rho(t)$ is the microflake density and $\sigma(\omega_o)$ is the projected area, maintaining the consistency. Figure 3 compares the transmittance of our generalized macrofacet and an isotropic GPIS. When the travel distance t increases, there will be a slight difference with the transmittance of the GPIS. We believe that it is because of the de-correlation to simply calculate the extinction coefficient. However, if we don’t assume the independence, the extinction coefficient will depend on the origin of the ray, making macrofacet not a typical medium.

Phase function. Because the GPIS is not a height field any more, some equivalences in microfacet theory are no longer applicable, such as NDF [Heitz 2014]:

$$\int_{H^2} \langle \omega_m, \omega_g \rangle D(\omega_m) d\omega_m = 1. \quad (21)$$

When the GPIS is not a height field, its normals distribute on the full sphere instead of the hemisphere. Also, there are overlaps making the integration on left hand side bigger than 1. Therefore, we must carefully consider the nature of NDF. Recall the definition of NDF [Walter et al. 2007]: NDF multiplied by an infinitesimal solid angle $d\omega_m$ centered on ω_m and an infinitesimal macro-surface area dA is the total area of the portion of the corresponding micro-surface whose normals lie within $d\omega_m$. NDF is the area of micro-surface, so we can connect gradient distribution function (GDF) to NDF using the following equation:

$$D(\omega_m) = \int_0^\infty P(g)t^3 dt, \quad (22)$$

where the gradient $g = t\omega_m$, and $P(g)$ is the probability density function of gradients. This equation is straight forward - the area of micro-surface whose normal is ω_m is the sum of the area of gradients which lie on ω_m . The area of a gradient g is t , and t^2 is Jacobian. Within this equation, we establish the connection between GDF and NDF. It does not depend on Gaussian processes. It is applicable for any GDF, and also SDF distribution.

Next we need to know about GDF. Within the independent assumption we make in the transmittance calculation, we do not need to consider other points but the current point \mathbf{x}_0 on the ray. Therefore, the distribution $P(g(\mathbf{x}_0) | f(\mathbf{x}_0) = 0)$ of gradient $g(\mathbf{x}_0)$

conditioned on $f(\mathbf{x}_0) = 0$ is a Gaussian distribution:

$$g' \sim \mathcal{N}\left((0, 0, 1)^T, \sigma^2 \text{diag}(l_x^2, l_y^2, l_z^2)^{-1}\right), \quad (23)$$

where we simplify the notation $g(\mathbf{x}_0) | f(\mathbf{x}_0) = 0$ as g' . We insert it into Equation 22. After simplification we mention in the supplemental material, we can get

$$\begin{aligned}D(\omega_m) &= \frac{e^{-C+B^2/A}}{\pi^{3/2}\alpha_x\alpha_y\alpha_z} \left[\frac{1}{2A^2} \left(\frac{B^2}{A} + 1 \right) e^{-B^2/A} \right. \\ &\quad \left. + \frac{B\sqrt{\pi}}{2A^{5/2}} \left(\frac{B^2}{A} + \frac{3}{2} \right) \text{erfc} \left(-\frac{B}{\sqrt{A}} \right) \right], \\ A &= \frac{\sin^2 \theta_m \cos^2 \phi_m}{\alpha_x^2} + \frac{\sin^2 \theta_m \sin^2 \phi_m}{\alpha_y^2} + \frac{\cos^2 \theta_m}{\alpha_z^2}, \\ B &= \frac{\cos \theta_m}{\alpha_z^2}, \\ C &= \frac{1}{\alpha_z^2},\end{aligned}\quad (24)$$

where erfc is the complementary error function. When $\alpha_z \rightarrow 0$, that is, $l_z \rightarrow \infty$, Equation 24 degenerates to the Beckmann NDF. Interestingly, some equivalences about NDF in microfacet theory still hold. For example, the signed projected area of the micro-surface is the same as the projected area of the macro-surface for any direction ω :

$$\int_{\Omega} (\omega \cdot \omega_m) D(\omega_m) d\omega_m = (\omega \cdot \omega_m). \quad (25)$$

We show this equivalence in the supplemental material. This ensures that the surface is manifold.

As we have the analytical solution for NDF, we can compute vNDF using Equation 11 so as to compute the phase function using Equation 10. However, the normalized factor in the denominator is still a problem. In fact, it is equal to the projected area listed in Equation 19. We show this equivalence in Figure 5. This maintains the consistency with microflake theory and the reciprocity of phase function. We compare our vNDF with the one generated by GPIS [Seyb et al. 2024] in Figure 6, showing the great consistency.

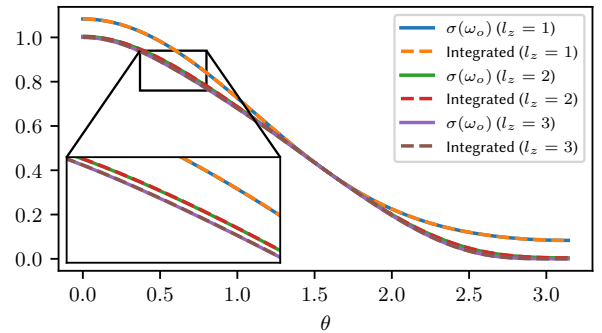


Fig. 5. The equivalence between the normalized factor in vNDF and projected area. We compare the normalized factor computed by numerical integration (orange, red and brown lines) and the projected area $\sigma(\omega_o)$ in Equation 19 (blue, green and purple lines) with different correlation on the z -axis l_z . The normalized factor matches projected area well whatever l_z is.

Importance sampling this vNDF is a difficult problem due to the error function making it unable to use inverse methods. For now, we combine Beckmann vNDF importance sampling [Heitz and d'Eon 2014] with ratio R and uniform hemisphere whose z -axis is $-\omega_o$ sampling with ratio $1 - R$ to sample ω_m .

5 RESULTS

We implemented our macrofacet in PBRT [Pharr et al. 2016]. We ran all experiments with an Intel Core i9-9900K CPU. We adopted null-scattering [Miller et al. 2019] as our volumetric rendering method. We use mean squared error (MSE) to evaluate the difference between rendering results and references. Our results show high quality renderings at a low time cost. We show macrofacet with different parameter settings in Figure 11.

5.1 Comparisons with Microfacet

We compare Beckmann macrofacet with Beckmann microfacet in Figure 7. We set the variance $\sigma = 0.01$ to limit the length of the shell like a surface. The roughness changes from 0.1 to 1.0. We render results in both single-scattering and multiple-scattering. The multiple-scattering Beckmann microfacet is implemented from Cui et al. [2023]. The results show that macrofacet is consistent with microfacet in both single scattering and multiple scattering. It also means that macrofacet supports multiple-scattering microfacet naturally because it is rendered as a volume. We also compare GGX macrofacet with GGX microfacet in Figure 10. We can see that no matter what NDF is chosen, our macrofacet is fit with microfacet when it degenerates to a surface. Besides, Figure 10 shows how the appearance of macrofacet changes when the variance σ grows up. We proceed to compare anisotropic generalized macrofacet and isotropic generalized macrofacet in Figure 13, showing the impact of correlation on the z -axis.

5.2 Comparisons with Gaussian Processes

We compare generalized macrofacet with isotropic GPISes proposed by Seyb et al. [2024] and Xu et al. [2025] with different variance and roughness. All GPISes use squared exponential kernel as their covariance kernel. We keep the variance and roughness of GPISes the same as macrofacet. We first verify whether macrofacet appears similar with GPIS with different pairs of variance and roughness. Figure 12 shows that no matter what variance and roughness it is, macrofacet appears similar with GPIS.

We render generalized macrofacet and GPISes at the same time (100 seconds) in Figure 14. The result shows that macrofacet is significantly faster than GPISes and can render more samples per pixel (spp) at the same time because it is realization free. We note that there is a slight difference with the one rendered by GPIS approach at the sharp area of geometry. This is because the different independent assumption we make in order to convert GPISes into classic exponential media, as we discussed in Section 6. Moreover, we compare generalized macrofacet with a spatially variant GPIS in Figure 1. Our macrofacet still outperform previous work in rendering time and maintain a similar appearance.

6 DISCUSSION

Independent assumptions. Both macrofacet and previous GPIS approaches [Seyb et al. 2024; Xu et al. 2025] make different relaxations to deal with dependency because of correlation. Previous GPIS approaches march rays segment by segment. Because a realization of Gaussian process conditioned on the entire path costs unacceptable time, they propose Renewal and Renewal+ models. The Renewal model only conditions on the SDF of previous intersection, while the Renewal+ model conditions on the SDF and gradient of previous intersection. In other words, they both make an assumption that the current realization is independent on earlier segments and intersections. Macrofacet is neither Renewal nor Renewal+ model. We assume that SDF and gradient at the current point are independent with those at the origin point of ray. The difference is shown in Figure 8. Because of this, we do not expect exactly the same result. We believe that macrofacet is promising to handle full path correlation if we introduce non-classic media.

Non-classic media. GPIS cannot be represented as a classic exponential medium essentially because of correlation. Correlation makes the volumetric properties, such as the extinction coefficient, of current point depends on the origin point of ray, as discussed in Section 4.2. As a result, the transmittance is not multiplicative along points on a ray, where $\text{Tr}(x \rightarrow y) \neq \text{Tr}(x \rightarrow z)\text{Tr}(z \rightarrow y)$, as shown in Figure 9. To deal with correlation, non-exponential media may be used [Bitterli et al. 2018; Jarabo et al. 2018]. However, we hope to stick to classic exponential media so that macrofacet can be applicable for commonly used rendering engines.

Normal distribution. Inspired by the definition of NDF, we propose the area of GDF in Equation 22 to compute NDF. This is independent with Gaussian processes. Furthermore, within the independent assumption, we can use SDF distribution to define micro-geometry and convert any stochastic processes implicit surface to macrofacet if we know the GDF and SDF distribution of any point in the space.

7 CONCLUSION AND FUTURE WORK

We present macrofacet theory. We extend a macro-surface to a volume according to the variance and convert microfacet theory into microflake theory in macro-space. Within macrofacet theory, microfacet theory is connected to the GPIS. In order to support correlation on the z -axis, which we call generalized macrofacet, we apply an independent assumption to compute the extinction coefficient and phase function. As a consequence, we can render appearance of GPIS by classic exponential media rendering methods to accomplish a faster convergence speed. Moreover, artists can choose different typical normal distributions to realize the appearance they want without understanding principles of Gaussian processes.

In the future, we would use non-exponential media to represent GPIS to solve correlation problems like non-multiplicative transmittance and full spherical visible normals' distribution. Besides, since noise is produced from volumetric rendering, which has extensive research instead of GPIS, we would implement denoising techniques to further improve our convergence in order to achieve real-time rendering. In addition, we would try to use importance sampling to sample vNDF of generalized macrofacet. Moreover, we only focus

on the conductor material in this paper, so we would discover the dielectric material later.

References

- P. Beckmann. 1965. Shadowing of random rough surfaces. *IEEE Transactions on Antennas and Propagation* 13, 3 (1965), 384–388. doi:10.1109/TAP.1965.1138443
- Benedikt Bitterli and Eugene d'Eon. 2022. A Position-Free Path Integral for Homogeneous Slabs and Multiple Scattering on Smith Microfacets. *Computer Graphics Forum* 41, 4 (2022), 93–104. arXiv:https://onlinelibrary.wiley.com/doi/pdf/10.1111/cgf.14589 doi:10.1111/cgf.14589
- Benedikt Bitterli, Srinath Ravichandran, Thomas Müller, Magnus Wrenninge, Jan Novák, Steve Marschner, and Wojciech Jarosz. 2018. A radiative transfer framework for non-exponential media. *ACM Trans. Graph.* 37, 6, Article 225 (Dec. 2018), 17 pages. doi:10.1145/3272127.3275103
- R. L. Cook and K. E. Torrance. 1982. A Reflectance Model for Computer Graphics. *ACM Trans. Graph.* 1, 1 (Jan. 1982), 7–24. doi:10.1145/357290.357293
- Yuang Cui, Gaole Pan, Jian Yang, Lei Zhang, Ling-Qi Yan, and Beibei Wang. 2023. Multiple-bounce Smith Microfacet BRDFs using the Invariance Principle. In *SIGGRAPH Asia 2023 Conference Papers* (Sydney, NSW, Australia) (SA '23). Association for Computing Machinery, New York, NY, USA, Article 39, 10 pages. doi:10.1145/3610548.3618198
- Jonathan Dupuy, Eric Heitz, and Eugene d'Eon. 2016. Additional progress towards the unification of microfacet and microflake theories. In *Proceedings of the Eurographics Symposium on Rendering: Experimental Ideas & Implementations* (Dublin, Ireland) (EGSR '16). Eurographics Association, Goslar, DEU, 55–63.
- Eric Heitz. 2014. Understanding the Masking-Shadowing Function in Microfacet-Based BRDFs. *Journal of Computer Graphics Techniques (JCGT)* 3, 2 (30 June 2014), 48–107. http://jcggt.org/published/0003/02/03/
- E. Heitz and E. d'Eon. 2014. Importance Sampling Microfacet-Based BSDFs using the Distribution of Visible Normals. *Computer Graphics Forum* 33, 4 (2014), 103–112. arXiv:https://onlinelibrary.wiley.com/doi/pdf/10.1111/cgf.12417 doi:10.1111/cgf.12417
- Eric Heitz, Jonathan Dupuy, Cyril Crassin, and Carsten Dachsbacher. 2015. The SGGX microflake distribution. *ACM Trans. Graph.* 34, 4, Article 48 (July 2015), 11 pages. doi:10.1145/2766988
- Eric Heitz, Johannes Hanika, Eugene d'Eon, and Carsten Dachsbacher. 2016. Multiple-scattering microfacet BSDFs with the Smith model. *ACM Trans. Graph.* 35, 4, Article 58 (July 2016), 14 pages. doi:10.1145/2897824.2925943
- Wenzel Jakob, Adam Arbree, Jonathan T. Moon, Kavita Bala, and Steve Marschner. 2010. A radiative transfer framework for rendering materials with anisotropic structure. *ACM Trans. Graph.* 29, 4, Article 53 (July 2010), 13 pages. doi:10.1145/1778765.1778790
- Adrian Jarabo, Carlos Aliaga, and Diego Gutierrez. 2018. A radiative transfer framework for spatially-correlated materials. *ACM Trans. Graph.* 37, 4, Article 83 (July 2018), 13 pages. doi:10.1145/3197517.3201282
- James T. Kajiya. 1986. The rendering equation. *SIGGRAPH Comput. Graph.* 20, 4 (Aug. 1986), 143–150. doi:10.1145/15886.15902
- I. Kušćer and G. C. Summerfield. 1969. Symmetries in Scattering of Slow Neutrons. *Phys. Rev.* 188 (Dec 1969), 1445–1449. Issue 3. doi:10.1103/PhysRev.188.1445
- Wolfram Martens, Yannick Poffet, Pablo Ramón Soria, Robert Fitch, and Salah Sukkarieh. 2017. Geometric Priors for Gaussian Process Implicit Surfaces. *IEEE Robotics and Automation Letters* 2, 2 (2017), 373–380. doi:10.1109/LRA.2016.2631260
- Bailey Miller, Iliyan Georgiev, and Wojciech Jarosz. 2019. A null-scattering path integral formulation of light transport. *ACM Trans. Graph.* 38, 4, Article 44 (July 2019), 13 pages. doi:10.1145/3306346.3323025
- Matt Pharr, Wenzel Jakob, and Greg Humphreys. 2016. *Physically Based Rendering: From Theory to Implementation* (3rd ed.). Morgan Kaufmann Publishers Inc., San Francisco, CA, USA.
- Carl Edward Rasmussen and Christopher K. I. Williams. 2005. *Gaussian Processes for Machine Learning*. The MIT Press. arXiv:https://direct.mit.edu/book-pdf/2514321/book_9780262256834.pdf doi:10.7551/mitpress/3206.001.0001
- Luigi M. Ricciardi and Shunsuke Sato. 1986. On the evaluation of first passage time densities for Gaussian processes. *Signal Processing* 11, 4 (1986), 339–357. doi:10.1016/0165-1684(86)90076-9
- Kai Schröder, Shuang Zhao, and Arno Zinke. 2012. Recent advances in physically-based appearance modeling of cloth. In *SIGGRAPH Asia 2012 Courses* (Singapore, Singapore) (SA '12). Association for Computing Machinery, New York, NY, USA, Article 12, 52 pages. doi:10.1145/2407783.2407795
- Dario Seyb, Eugene d'Eon, Benedikt Bitterli, and Wojciech Jarosz. 2024. From microfacets to participating media: A unified theory of light transport with stochastic geometry. *ACM Trans. Graph.* 43, 4, Article 112 (July 2024), 17 pages. doi:10.1145/3658121
- B. Smith. 1967. Geometrical shadowing of a random rough surface. *IEEE Transactions on Antennas and Propagation* 15, 5 (1967), 668–671. doi:10.1109/TAP.1967.1138991
- Jos Stam. 2001. An illumination model for a skin layer bounded by rough surfaces. In *Proceedings of the 12th Eurographics Conference on Rendering* (London, UK) (EGWR'01). Eurographics Association, Goslar, DEU, 39–52.
- T. S. Trowbridge and K. P. Reitz. 1975. Average irregularity representation of a rough surface for ray reflection. *J. Opt. Soc. Am.* 65, 5 (May 1975), 531–536. doi:10.1364/JOSA.65.000531
- H. C. van de Hulst. 1957. *Light Scattering by Small Particles*. John Wiley & Sons.
- Bruce Walter, Stephen R. Marschner, Hongsong Li, and Kenneth E. Torrance. 2007. Microfacet models for refraction through rough surfaces. In *Proceedings of the 18th Eurographics Conference on Rendering Techniques* (Grenoble, France) (EGSR'07). Eurographics Association, Goslar, DEU, 195–206.
- Beibei Wang, Wenhua Jin, Jiahui Fan, Jian Yang, Nicolas Holzschuch, and Ling-Qi Yan. 2022. Position-free multiple-bounce computations for smith microfacet BSDFs. *ACM Trans. Graph.* 41, 4, Article 134 (July 2022), 14 pages. doi:10.1145/3528223.3530112
- M. M. R. Williams. 1978. Transport theory in anisotropic media. *Mathematical Proceedings of the Cambridge Philosophical Society* 84, 3 (1978), 549–567. doi:10.1017/S0305004100055377
- Oliver Williams and Andrew Fitzgibbon. 2007. Gaussian Process Implicit Surfaces. In *Gaussian Processes in Practice* (gaussian processes in practice ed.). https://www.microsoft.com/en-us/research/publication/gaussian-process-implicit-surfaces-2/
- Kehan Xu, Benedikt Bitterli, Eugene d'Eon, and Wojciech Jarosz. 2025. Practical Gaussian Process Implicit Surfaces with Sparse Convolutions. *ACM Trans. Graph.* 44, 6, Article 188 (Dec. 2025), 18 pages. doi:10.1145/3763329
- Shuang Zhao, Wenzel Jakob, Steve Marschner, and Kavita Bala. 2011. Building volumetric appearance models of fabric using micro CT imaging. *ACM Trans. Graph.* 30, 4, Article 44 (July 2011), 10 pages. doi:10.1145/2010324.1964939
- Shuang Zhao, Wenzel Jakob, Steve Marschner, and Kavita Bala. 2012. Structure-aware synthesis for predictive woven fabric appearance. *ACM Trans. Graph.* 31, 4, Article 75 (July 2012), 10 pages. doi:10.1145/2185520.2185571

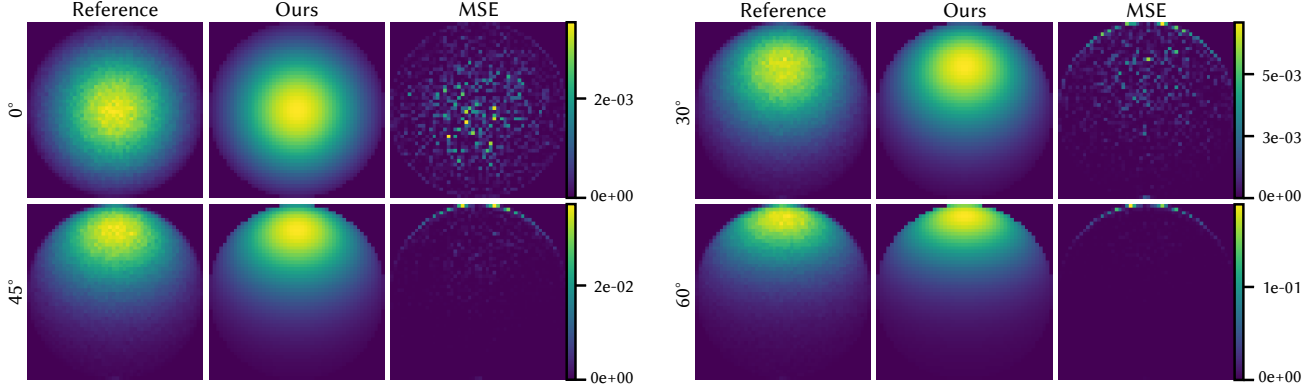


Fig. 6. We compare our vNDF with the one generated by GPIS at different incident angles. The first and fourth columns are vNDF generated by GPIS. The second and fifth columns are our vNDF. The third and sixth columns are MSE between our vNDF and the one generated by GPIS. From left to right, from top to bottom, incident angles are 0° , 30° , 45° and 60° , respectively. The roughness on all axes are 1.0. MSE shows that our vNDF matches the reference accurately.

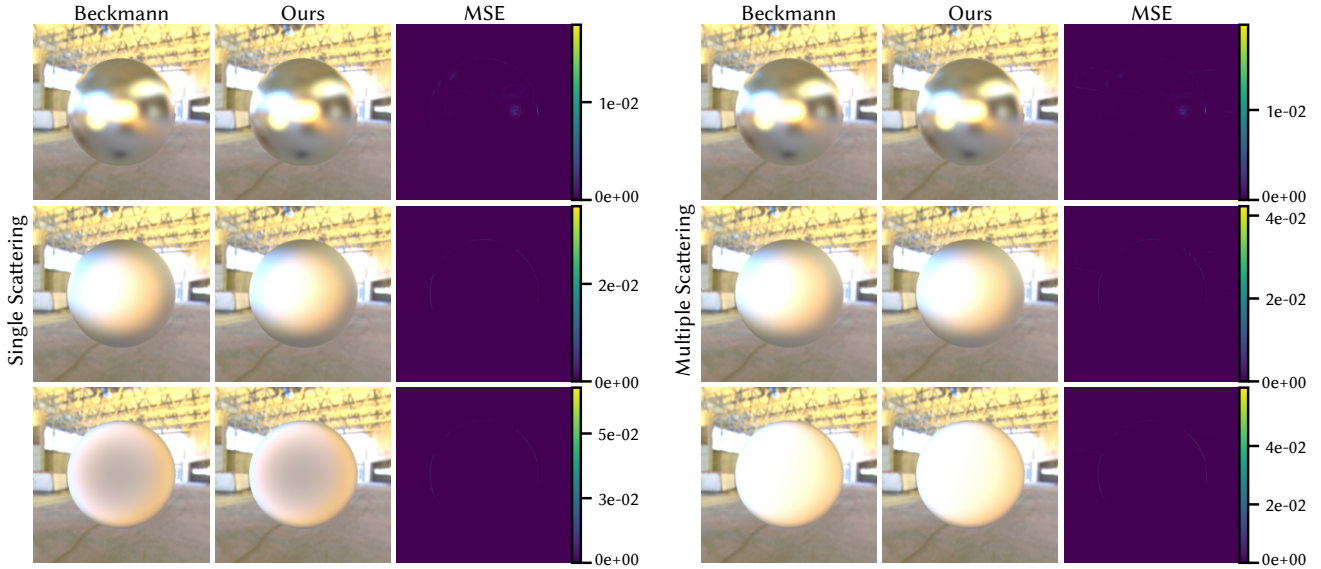


Fig. 7. Comparisons between Beckmann macrofacet and Beckmann microfacet with different roughness. The first column is single-scattering Beckmann microfacet. The second column is single-scattering Beckmann macrofacet. The third column is MSE between the first and second columns. The fourth column is multiple-scattering Beckmann microfacet. The fifth column is multiple-scattering Beckmann macrofacet. The sixth is MSE between the fourth and fifth columns. From top to bottom, the roughness are 0.1, 0.5 and 1.0, respectively. MSE shows that macrofacet is consistent with microfacet.

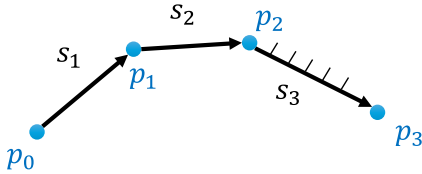


Fig. 8. Different independent assumptions between macrofacet and GPIS approaches. A path consists of three segments s_1 , s_2 , s_3 , and four intersections p_0 , p_1 , p_2 , p_3 . When GPIS approaches [Seyb et al. 2024; Xu et al. 2025] ray march the last segment s_3 , they only depend on the previous intersection p_2 and ignore earlier segments s_1 , s_2 and intersections p_0 , p_1 . Macrofacet is independent on all other segments and intersections except the current intersection p_3 .

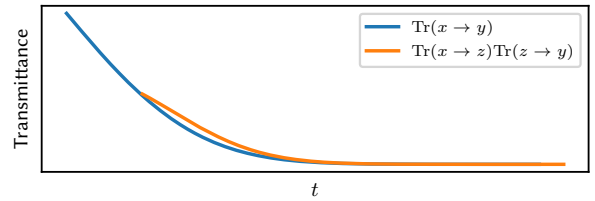


Fig. 9. We show two lines of transmittance of GPIS started from x (blue line) and z (orange line). And we multiply the transmittance started from z by the transmittance $\text{Tr}(x \rightarrow z)$ from x to z . For any point y after z , we can see that these two lines do not match, which means that the transmittance is not multiplicative: $\text{Tr}(x \rightarrow y) \neq \text{Tr}(x \rightarrow z)\text{Tr}(z \rightarrow y)$.

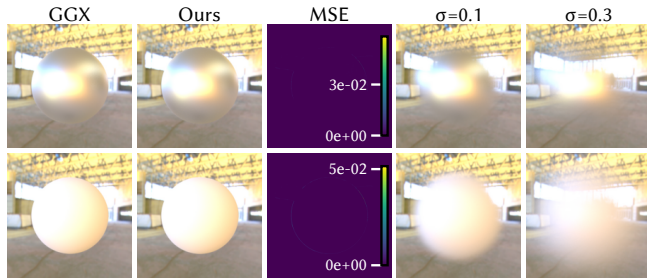


Fig. 10. Comparisons between GGX macrofacet and GGX microfacet with different roughness. The first column is multiple-scattering GGX microfacet. The second column is multiple-scattering GGX macrofacet. The third column is MSE between the first and second column. The fourth column is GGX microfacet with variance $\sigma = 0.1$. The fifth column is GGX microfacet with variance $\sigma = 0.3$. From top to bottom, the roughness are 0.2 and 0.8, respectively. MSE shows that macrofacet can adapt to different NDF.

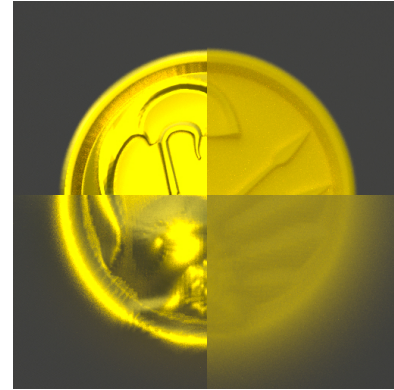


Fig. 11. Macrofacet with different variance and correlation. From left to right, from top bottom, pairs of variance and roughness (σ, α) are $(0.01, 0.1)$, $(0.01, 1)$, $(0.2, 0.1)$ and $(0.2, 1)$, respectively.

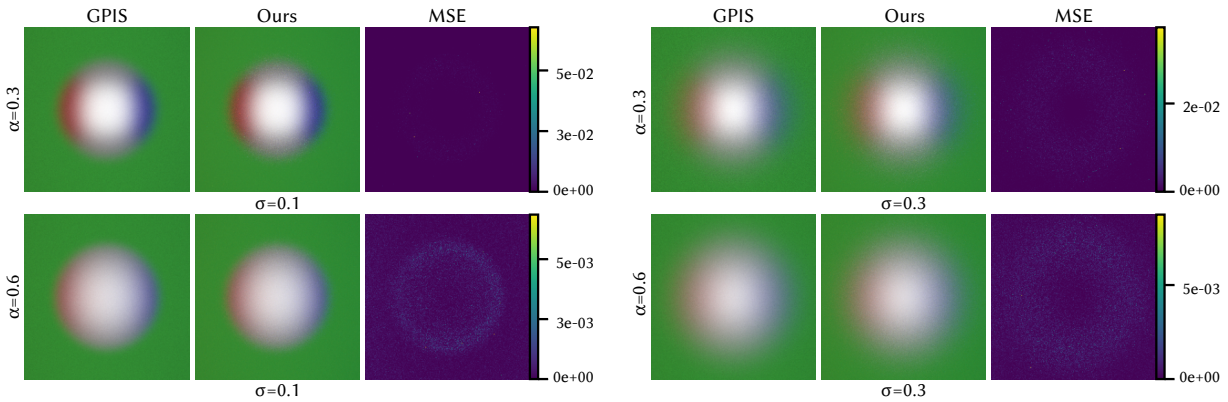


Fig. 12. Comparisons between macrofacet and GPISes with different pairs of variance and roughness. The first and fourth columns are GPISes. The second and fifth columns are macrofacet. The third and sixth columns are MSE between macrofacet and GPISes. From left to right, from top to bottom, pairs of variance and roughness (σ, α) are $(0.1, 0.3)$, $(0.3, 0.3)$, $(0.1, 0.6)$ and $(0.3, 0.6)$, respectively. MSE shows that macrofacet preserves statistical consistency with GPIS.



Fig. 13. Comparisons between anisotropic generalized macrofacet (top) and isotropic generalized macrofacet (bottom). For anisotropic one, $\alpha_z = 0.1$. For isotropic one, $\alpha_z = 1$. The highlight shows the impact of correlation on the z -axis.

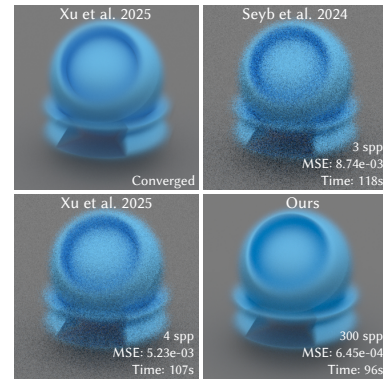


Fig. 14. Comparisons between macrofacet and GPISes at the same time. From left to right, from top to bottom, the first and third images are rendered by Xu et al. [2025]. The second image is rendered by Seyb et al. [2024]. The fourth images is rendered by our approach. We keep the second to fourth images the same time. It shows that macrofacet coverages much faster than others.